Gate-Tunable Berry Curvature Dipole Polarizability in Dirac Semimetal Cd$_3$As$_2$

Tong-Yang Zhao, An-Qi Wang,[*] Xing-Guo Ye, Xing-Yu Liu, Xin Liao [●], and Zhi-Min Liao [●][†]

State Key Laboratory for Mesoscopic Physics and Frontiers Science Center for Nano-optoelectronics, School of Physics,
Peking University, Beijing 100871, China and Hefei National Laboratory, Hefei 230088, China

We reveal the gate-tunable Berry curvature dipole polarizability in Dirac semimetal Cd$_3$As$_2$ nanoplates through measurements of the third-order nonlinear Hall effect. Under an applied electric field, the Berry curvature exhibits an asymmetric distribution, forming a field-induced Berry curvature dipole, resulting in a measurable third-order Hall voltage with a cubic relationship to the longitudinal electric field. Notably, the magnitude and polarity of this third-order nonlinear Hall effect can be effectively modulated by gate voltages. Furthermore, our scaling relation analysis demonstrates that the sign of the Berry curvature dipole polarizability changes when tuning the Fermi level across the Dirac point, in agreement with theoretical calculations. The results highlight the gate control of nonlinear quantum transport in Dirac semimetals, paving the way for promising advancements in topological electronics.

The concepts of Berry connection and Berry curvature play essential roles in the development of modern topological physics [1–10]. The quantized topological quantities, such as charge polarization [3], integer quantum Hall conductance [4,11], and magnetoelectric polarizability [9], can be expressed as the integrals of Berry connection. The Berry curvature and Berry curvature dipole (BCD) are responsible for the linear and second-order anomalous Hall effects, respectively, [12–24]. The first-order anomalous Hall effect occurs in materials with broken time-reversal symmetry; while the second-order anomalous Hall effect can occur in materials with time-reversal symmetry, but it usually requires the breaking of inversion symmetry. Even that both time-reversal symmetry and spatial inversion symmetry are present, the third-order anomalous Hall effect can still be observed, which arises from the Berry connection polarization effect [25–30]. Under an electric field, the Berry connection polarizability (BCP) can lead to a BCD, which further results in the third-harmonic anomalous Hall signals with respect to the biased alternating electric field. The third-order nonlinear Hall effect provides an effective method to study the Berry connection polarization effect and the field-induced BCD in nonmagnetic materials with inversion symmetry.

The Dirac semimetal provides an ideal platform to investigate the Berry connection and Berry curvature related effects. Dirac semimetals are featured with inverted band structures and massless Dirac fermions [31–33], which inherit nontrivial Berry phase and invoke exotic transport phenomena, such as chiral anomaly [34–36], and Shubnikov–de Haas oscillations with Berry phase π [37–40]. Despite extensive studies evidencing the nontrivial topological origin, the direct investigation on Berry parameters remains elusive in Dirac semimetals up to now. Here, we study the BCD polarization effect in the Dirac semimetal Cd$_3$As$_2$ nanoplate by combining theoretical calculations and experimental measurements. Theoretical calculations show that in the presence of an electric field, the induced BCD strongly depends on the chemical potential, and reverses its sign as across the Dirac point. Experimentally, we employ the measurements of third-order nonlinear Hall signal to probe the electric field-induced BCD for various gate voltages and temperatures.

The third-order nonlinear Hall effect in nonmagnetic materials is closely associated with BCP tensor $\overset{\leftrightarrow}{G}$, which is gauge invariant and represents an intrinsic band geometric property [27,28]. The BCP tensor elements are given as $G_{\alpha\beta} = 2e\Re \sum_{m\neq n}[(\mathcal{A}_\alpha)_{mn}(\mathcal{A}_\beta)_{nm}/\varepsilon_n - \varepsilon_m]$, where α, β denote the spatial direction, e is the electron charge, $(\mathcal{A}_\alpha)_{mn} = \langle u_m|i\partial_{k_\alpha}|u_n\rangle$ represents the interband Berry connection, and ε_n is the band energy. Under the presence of an electric field $\boldsymbol{E}$ and BCP, the Berry connection is generated as $\mathbf{A}^E = \overset{\leftrightarrow}{G} \cdot \mathbf{E}$, which further leads to a field-induced Berry curvature $\boldsymbol{\Omega}^E = \nabla_k \times \mathbf{A}^E$ and thereby the field-induced BCD (D^E). The D^E together with the applied field $\boldsymbol{E}$ would lead to the nonlinear Hall effect as the third-order Hall response, in which the third-harmonic Hall voltage depends on the cube of longitudinal electric field. Although the third-order nonlinear Hall effect associated with BCD polarization has been experimentally observed [27–30], the relationship between this BCD polarization and the variation of the Fermi energy level has not been revealed in experiments yet. In the following, we first theoretically calculate the BCP tensor and BCD polarizability at different chemical potentials for the Dirac semimetal Cd$_3$As$_2$. The BCD polarizability is defined as the ratio between D^E and the amplitude of $\boldsymbol{E}$, which is a sample-intrinsic quantity (Supplemental Material Note 1 [41]).
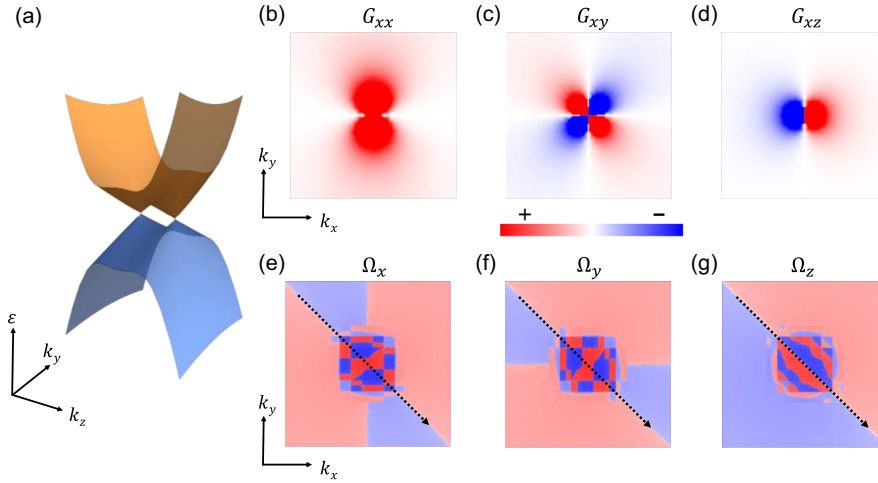
FIG. 1.   Numerical analysis of the Berry connection polarizability tensor and Berry curvature of a Dirac semimetal. (a) Bulk dispersion of Cd_3As_2 calculated from 4-band effective model, plotted in the $k_x = 0$ plane. A pair of Dirac points along the $\Gamma - Z$ direction can be found at the band intersections. (b)–(d) Sectional plots of representative tensor elements of BCP tensor $\overleftrightarrow{G}$ with respect to k_x and k_y, with $k_z = k_D$ specifically chosen to let the sectional plane go across the Dirac point. (e)–(g) The electric field-induced Berry curvature $\mathbf{\Omega}$ distribution in the same sectional plane as in (b)–(d). The bias electric field is chosen to point to the $[1\bar{1}0]$ direction as illustrated by the dashed arrows.

We start our theoretical analysis of Dirac semimetal Cd_3As_2 from the typical four-band effective model [31]. With the obtained energy dispersion [Fig. 1(a)] and corresponding wavefunctions, we can derive the BCP tensor elements related to the nonlinear response. Figures 1(b)–1(d) present the distribution of BCP tensor elements in the $k_z = k_D$ plane of momentum space, where $(0, 0, \pm k_D)$ are the positions of two Dirac points. Because of the 3D nature of Dirac semimetal, the calculation is extended to the BCP component with index z besides the common index x, y for 2D materials. As we can see, the BCP is concentrated around the Dirac point region. We introduce an electric field oriented along the $[1\bar{1}0]$ direction, which is the actual direction of applied electric field in our experiment, and calculate the resultant Berry curvature distribution, as shown in Figs. 1(e)–1(g). The induced BCD can be calculated by the dipole moment formula $D_{\alpha\beta} = \int_k dk\, f_0(\partial_{k_\alpha}\Omega_\beta)$, where f_0 is the equilibrium distribution function and the integration is taken over the Brillouin zone [44]. Then one can deduce the nonlinear current along the in-plane transverse direction (Supplemental Material Note 1 [41]), that is the nonlinear Hall current $j_\perp^{NL}$. In a 3D system, the BCD is a rank-2 tensor which is hard to clarify and quantify, posing challenges in determining the dipole from experimental conditions. Intuitively, we introduce the concept of effective BCD (Supplemental Material Note 1 [41]). The effective scalar value of BCD in the Cd_3As_2 nanoplate can be calculated by dividing the Hall current $j_\perp^{NL}$ with a $|\mathbf{E}|^2$ term, similar to the case of 2D systems [19]. We obtain the effective BCD under various chemical potentials [Fig. 4(d)]. It is found that the field-induced BCD is sensitive to the variation of chemical potential, and even switches its

sign across the Dirac point. In other words, the field polarizability of BCD strongly depends on the Fermi level position for the Dirac semimetal Cd_3As_2.

We carry out low temperature electric transport measurements to reveal the BCD polarization of Dirac semimetal Cd_3As_2. The Cd_3As_2 nanoplates were grown by chemical vapor deposition (CVD) method with (112) surface plane and $[1\bar{1}0]$ edge direction [45,46]. Nanoplates with thickness of ~ 80 nm were selected and mechanically transferred onto the SiO_2/Si substrate, which serves as the back gate to tune the sample Fermi level. Ti/Au electrodes were fabricated via electron beam evaporation (EBE) process after an *in situ* Ar ion etching treatment. All transport measurements were performed in a commercial Oxford cryostat. We here mainly discuss the results measured from device A, as shown in Fig. 2(a).

To measure the nonlinear Hall effect, we applied an ac driving current along the nanoplate edge direction [as indicated by the white arrow in Fig. 2(a)] at a fixed frequency of 17.777 Hz and recorded the longitudinal and transverse signals at the frequencies from the fundamental up to the third harmonics. At the fundamental frequency, the longitudinal voltage $V_\parallel$ increases linearly with the bias current $I_\parallel$. By contrast, the transverse voltage $V_\perp$ is vanishingly small as expected due to the preserved time-reversal symmetry in the Dirac semimetal. Figure 2(c) shows the detected second- and third-harmonic Hall voltage, i.e., $V_\perp^{2\omega}$ and $V_\perp^{3\omega}$, versus the applied bias current. The value of $V_\perp^{3\omega}$ is almost 3 times larger than that of $V_\perp^{2\omega}$ under $I_\parallel = 10\ \mu A$. For an ideal Dirac semimetal, the inversion symmetry is conserved in the bulk, which should result in the disappearance of second-order Hall response. However,
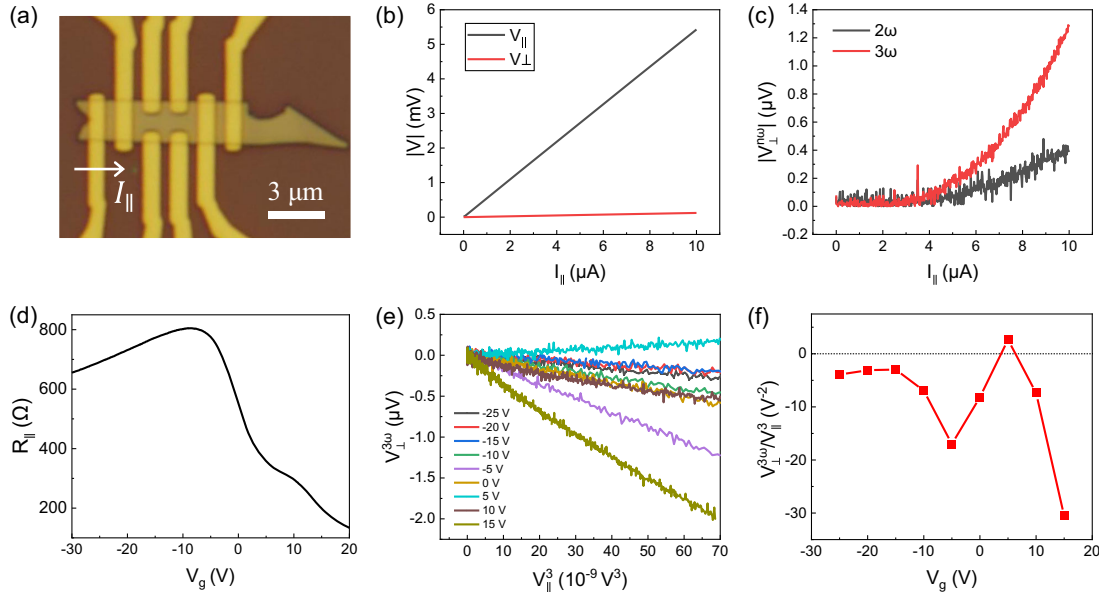
FIG. 2. Third-order nonlinear Hall effect observed in the Cd_3As_2 nanoplate. (a) Optical image of a typical Hall-bar device. An ac driving current $I_\parallel$ is applied along the nanoplate edge direction, whereas the longitudinal and transverse voltage are simultaneously recorded. (b) The first-harmonic longitudinal voltage $V_\parallel$ and transverse voltage $V_\perp$ as a function of bias longitudinal current $I_\parallel$. (c) Second- (black curve) and third-harmonic (red curve) $V_\perp^{n\omega}$ versus $I_\parallel$. (d) The transfer curve of the nanoplate, obtained from the standard four-probe measurement. (e) Third-harmonic Hall signal $V_\perp^{3\omega}$ scaled with the cube of longitudinal voltage $V_\parallel$ for various gate voltages. (f) The slope of $V_\perp^{3\omega}$ vs $V_\parallel^3$ as a function of gate voltage, which is found to be sensitive to V_g, and its amplitude reaches a local maximum near the Dirac point. The data were collected at 10 K.

in practical experiments, lattice symmetry-breaking may arise from factors such as strain introduced during device fabrication, differences in thermal expansion coefficient between the sample and substrate during the measurement cooling process, and surface atomic reconstruction. This lattice symmetry breaking can lead to a nonzero value of the $V_\perp^{2\omega}$ signal. The third-order Hall response takes the leading role in the nonlinear charge response. The third-order Hall signals are also independent of frequencies (Fig. S1 [41]), which excludes the possible measurement artifacts such as parasitic capacitance effect.

We then investigate the gate voltage dependence of third-order nonlinear Hall responses. The transfer curve [Fig. 2(d)] shows that the Dirac point of nanoplate is situated near $V_g = -10$ V. Figure 2(e) demonstrates that the third-harmonic transverse voltage scales linearly with the cube of first-harmonic $V_\parallel$ for all gate voltages. The slope of $V_\perp^{3\omega}$ versus $V_\parallel^3$ as a function of V_g is summarized in Fig. 2(f). As we can see, the $V_\perp^{3\omega}/V_\parallel^3$ is highly tunable by gate voltage, and its magnitude reaches a local maximum near the Dirac point. It is worth noting that this does not mean the field-induced BCD is the largest near the Dirac point. Generally, the $V_\perp^{3\omega}/V_\parallel^3$ involves the contributions from not only the field-induced dipole moment [27,28], but also the scattering process from disorders [42,43], which should be carefully considered.

The underlying mechanism of the nonlinear Hall effect is further investigated by studying its temperature dependence and scaling law behavior. Figure 3(a) gives the temperature dependence of third-order nonlinear Hall signals when the Fermi level situates in the conduction band ($V_g = 15$ V). The $V_\perp^{3\omega}$ exhibits a linear relation with the $V_\parallel^3$ for all temperatures. The slope of $V_\perp^{3\omega}$ vs $V_\parallel^3$ is gradually attenuated upon increasing the temperature as shown in Fig. 3(b). The conductance G also exhibits a similar temperature dependence [Fig. 3(c)]. Figure 3(d) gives the plot of $E_\perp^{3\omega}/E_\parallel^3$ as a function of σ/σ_0, where $(E_\perp^{3\omega}/E_\parallel^3) = (V_\perp^{3\omega}/V_\parallel^3) \cdot (L^3/W)$, $\sigma = G[L/(W \cdot t)]$, L, W, and t are the channel length, channel width, and nanoplate thickness, respectively. σ_0 refers to the conductivity at the base temperature 2 K. According to previous literature [42,43], the relation of $(E_\perp^{3\omega}/E_\parallel^3)$ and σ/σ_0 can be generally scaled as $(E_\perp^{3\omega}/E_\parallel^3) = A_0 + A_1(\sigma/\sigma_0) + A_2(\sigma/\sigma_0)^2$. Each of the scaling parameters A_0, A_1, and A_2 comes from the mixture of intrinsic and extrinsic contributions (Supplemental Material Note 4 [41]). The intrinsic contribution results from the Berry connection polarizability tensor and associates with the field-induced BCD. The extrinsic one stems from the disorder-related contributions, such as side jump and skew scatterings. As shown in Fig. 3(d), the parabolic scaling law can well fit the experimental data of $(E_\perp^{3\omega}/E_\parallel^3)$ versus (σ/σ_0).
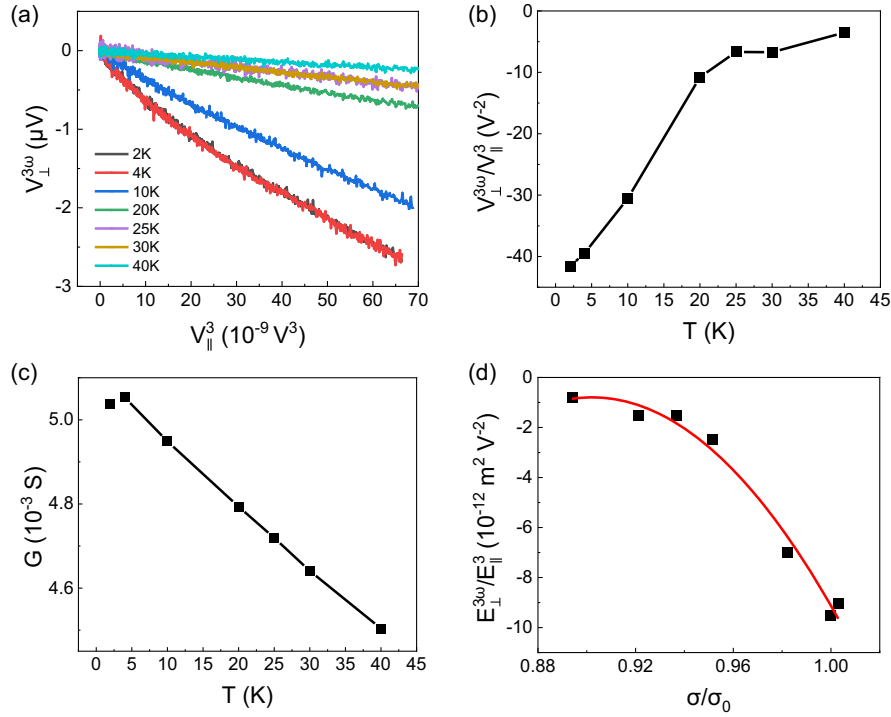
FIG. 3. Temperature dependence of third-order nonlinear Hall effect. (a) Third-order Hall signal $V_\perp^{3\omega}$ versus $V_\parallel$ for different temperatures. (b),(c) The slope of $V_\perp^{3\omega}$ vs $V_\parallel^3$ and nanoplate conductance G as a function of T, respectively. (d) $E_\perp^{3\omega}/E_\parallel^3$ versus σ/σ_0 in the Cd_3As_2 nanoplate. The square symbols represent experimental data. The lines in (b) and (c) are guides to the eye. The red solid curve in (d) is the fitting to the experimental data with the scaling formula. The data were acquired under $V_g = 15$ V.

To assess the relative contribution of different mechanisms, we carefully analyze the scaling parameters extracted from the parabolic fitting, as shown in Fig. 4(a) for the gate voltage dependence of A_0, A_1, and A_2. These three scaling parameters exhibit relatively unvaried ratio with $A_0 : A_1 : A_2 \approx 1 : -2 : 1$ in the whole range of gate voltage. Similar results are also obtained in another device (see the results of device B in Fig. S2 [41]). Since A_2 lacks any side-jump contribution, a dominant role of the side-jump mechanism would lead to A_0 and A_1 being significantly larger than A_2. However, this contradicts the fact that the observed amplitudes of the three parameters are similar. Consequently, the side-jump mechanism cannot be the primary factor influencing the scaling parameters. Besides, the high carrier mobility of Cd_3As_2 nanoplate also indicates the relative weak side jumps, which are usually pronounced in dirty metals [12]. For the similar reason, we can exclude the non-Gaussian skew scatterings as the main origin. Therefore, we obtain a simplified expression of scaling parameters as $A_0 = C_{11}^{sk,1} + C_{\text{int}}$, $A_1 = -2C_{11}^{sk,1}$, and $A_2 = C_{00}^{sk,1} + C_{11}^{sk,1}$. The parameter C_{int} denotes the intrinsic contribution following $C_{\text{int}} = (m^* e/2\hbar^2 n)\gamma$, where $\hbar$ is the reduced Plank constant, e is the electron charge, $m^* = 0.04m_e$ is the effective mass for Cd_3As_2, n is the carrier density, γ is the BCD polarizability defined as $\gamma = D/E$. The parameter $C_{00}^{sk,1}$ and $C_{11}^{sk,1}$ represent impurity- and

phonon-related Gaussian skew scatterings, respectively. Then we can obtain that $(E_\perp^{3\omega}/E_\parallel^3) = C_{\text{int}} + C_{00}^{sk,1}(\sigma/\sigma_0)^2 + C_{11}^{sk,1}[1-(\sigma/\sigma_0)]^2$, in which $C_{\text{int}} = A_0 + \frac{1}{2}A_1$, $C_{00}^{sk,1} = \frac{1}{2}A_1 + A_2$, and $C_{11}^{sk,1} = -\frac{1}{2}A_1$. The three terms on the right indicate the intrinsic contribution, impurity skew scattering contribution, phonon skew scattering contribution to the observed $(E_\perp^{3\omega}/E_\parallel^3)$.

Figure 4(b) shows the proportion of three types of mechanisms in contributing to the third-order nonlinear Hall effect. The intrinsic contribution and impurity skew scattering play a dominant role in the third-order nonlinear Hall effect. The contribution of phonon skew scattering is almost vanishing at low temperature ($T = 2$ K) due to the limited thermal activation. Upon increasing the temperature, the increased thermal activation induces more phonons and results in the enhanced phonon skew scattering [bottom panel of Fig. 4(b)]. Moreover, we have speculated the induced BCD under an electric field of $E = 1$ kV/m according to the relation $C_{\text{int}} = (m^* e/2\hbar^2 n)\gamma$, as shown in Fig. 4(c). At a fixed bias electric field, the induced dipole (charactering the dipole polarizability), is found to reverse its sign across the Dirac point and reaches a maximum value of 6 nm, 2 orders of magnitude larger than that in WTe_2 [29]. Both the sign reversal and maximum amplitude are consistent with the theoretical
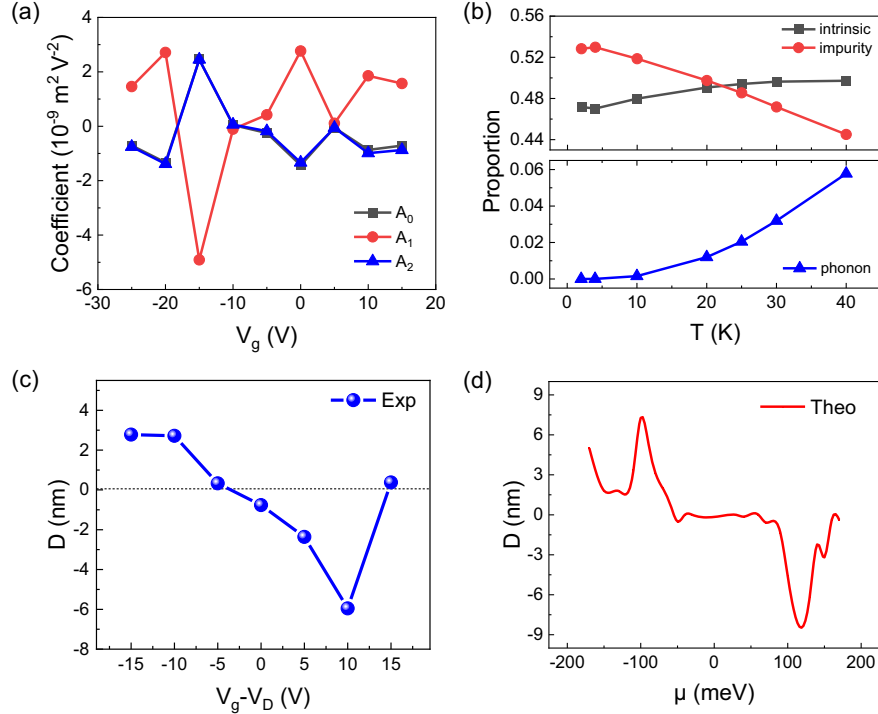
FIG. 4. Gate-tunable Berry curvature dipole observed in the Cd_3As_2 nanoplate. (a) Gate voltage dependence of three scaling parameters. (b) The proportion of three mechanisms, intrinsic contribution, impurity skew scattering, and phonon skew scattering in contributing to the third-order Hall effect. (c) The estimated BCD D versus gate voltage under a bias electric field of 1 kV/m. $V_D = -10$ V denotes the position of the Dirac point. (d) The theoretically calculated D as a function of chemical potential μ. The bias electric field is 1 kV/m.

results shown in Fig. 4(d), and the detailed comparisons are provided in Supplemental Material Note 5 [41].

To gain a deeper understanding of the connection between BCD polarizability and the energy band structure's topology, we conduct a numerical analysis on a conventional insulator model for comparison (see Supplemental Material Note 6 [41] for details). By merely deactivating band inversion and the corresponding band topology, we observe a substantial suppression of the electric field-induced BCD features (Fig. S3 [41]). This result indicates the important role of nontrivial topology in Dirac dispersion for achieving substantial BCD polarizability. In Dirac semimetals, the characteristic feature is the overlap of two Weyl points with opposite chirality at each Dirac point, leading to mutual cancellation of their Berry curvatures. Nevertheless, this "hidden" Berry curvature structure can be readily presented when the balance between the overlapping Weyl points is disrupted by applying an electric field to separate them in momentum space. This approach, which reveals hidden Berry curvature, holds great promise for exploring exotic physical properties in topological materials and their potential applications in devices.

In conclusion, we have systematically studied the third-order nonlinear Hall effect in the Dirac semimetal Cd_3As_2 nanoplate. The scaling relationship reveals that the third-order Hall effect is mainly contributed by the intrinsic contribution, i.e., electric field-induced BCD, and the extrinsic contribution, i.e., impurity skew scatterings. The BCD polarizability is found gate tunable, and changes its sign when the Fermi level crosses the Dirac point, in agreement with theoretical calculations. Our work reveals the BCD polarization effect in Dirac semimetals, enriching the understanding of nonlinear transport in topological semimetals.

[*]Corresponding author: anqi0112@pku.edu.cn
[†]Corresponding author: liaozm@pku.edu.cn

[1] M. V. Berry, Quantal phase factors accompanying adiabatic changes, Proc. R. Soc. A **392,** 45 (1984).
[2] F. Wilczek and A. Zee, Appearance of gauge structure in simple dynamical systems, Phys. Rev. Lett. **52,** 2111 (1984).
[3] R. D. Kingsmith and D. Vanderbilt, Theory of polarization of crystalline solids, Phys. Rev. B **47,** 1651 (1993).

[4] Y. Hatsugai, Chern number and edge states in the integer quantum Hall effect, Phys. Rev. Lett. **71**, 3697 (1993).

[5] M. C. Chang and Q. Niu, Berry phase, hyperorbits, and the Hofstadter spectrum, Phys. Rev. Lett. **75**, 1348 (1995).

[6] G. Sundaram and Q. Niu, Wave-packet dynamics in slowly perturbed crystals: Gradient corrections and Berry-phase effects, Phys. Rev. B **59**, 14915 (1999).

[7] D. Xiao, J. R. Shi, and Q. Niu, Berry phase correction to electron density of states in solids, Phys. Rev. Lett. **95**, 137204 (2005).

[8] M.-C. Chang and Q. Niu, Berry curvature, orbital moment, and effective quantum theory of electrons in electromagnetic fields, J. Phys. Condens. Matter **20**, 193202 (2008).

[9] A. M. Essin, J. E. Moore, and D. Vanderbilt, Magnetoelectric polarizability and axion electrodynamics in crystalline insulators, Phys. Rev. Lett. **102**, 146805 (2009).

[10] D. Xiao, M.-C. Chang, and Q. Niu, Berry phase effects on electronic properties, Rev. Mod. Phys. **82**, 1959 (2010).

[11] D. J. Thouless, M. Kohmoto, M. P. Nightingale, and M. Dennijs, Quantized Hall conductance in a two-dimensional periodic potential, Phys. Rev. Lett. **49**, 405 (1982).

[12] N. Nagaosa, J. Sinova, S. Onoda, A. H. MacDonald, and N. P. Ong, Anomalous Hall effect, Rev. Mod. Phys. **82**, 1539 (2010).

[13] Z. Z. Du, C. M. Wang, H.-Z. Lu, and X. C. Xie, Band signatures for strong nonlinear Hall effect in bilayer WTe$_2$, Phys. Rev. Lett. **121**, 266601 (2018).

[14] S.-Y. Xu, Q. Ma, H. Shen, V. Fatemi, S. Wu, T.-R. Chang, G. Chang, A. M. M. Valdivia, C.-K. Chan, Q. D. Gibson *et al.*, Electrically switchable Berry curvature dipole in the monolayer topological insulator WTe$_2$, Nat. Phys. **14**, 900 (2018).

[15] J.-S. You, S. Fang, S.-Y. Xu, E. Kaxiras, and T. Low, Berry curvature dipole current in the transition metal dichalcogenides family, Phys. Rev. B **98**, 121109(R) (2018).

[16] Y. Zhang, Y. Sun, and B. Yan, Berry curvature dipole in Weyl semimetal materials: An *ab initio* study, Phys. Rev. B **97**, 041101(R) (2018).

[17] Y. Zhang, J. van den Brink, C. Felser, and B. Yan, Electrically tuneable nonlinear anomalous Hall effect in two-dimensional transition-metal dichalcogenides WTe$_2$ and MoTe$_2$, 2D Mater. **5**, 044001 (2018).

[18] K. Kang, T. Li, E. Sohn, J. Shan, and K. F. Mak, Nonlinear anomalous Hall effect in few-layer WTe$_2$, Nat. Mater. **18**, 324 (2019).

[19] Q. Ma, S.-Y. Xu, H. Shen, D. MacNeill, V. Fatemi, T.-R. Chang, A. M. M. Valdivia, S. Wu, Z. Du, C.-H. Hsu *et al.*, Observation of the nonlinear Hall effect under time-reversal-symmetric conditions, Nature (London) **565**, 337 (2019).

[20] Z. Z. Du, H.-Z. Lu, and X. C. Xie, Nonlinear Hall effects, Nat. Rev. Phys. **3**, 744 (2021).

[21] S. Nandy and I. Sodemann, Symmetry and quantum kinetics of the nonlinear Hall effect, Phys. Rev. B **100**, 195117 (2019).

[22] L.-K. Shi and J. C. W. Song, Symmetry, spin-texture, and tunable quantum geometry in a WTe$_2$ monolayer, Phys. Rev. B **99**, 035403 (2019).

[23] S. Singh, J. Kim, K. M. Rabe, and D. Vanderbilt, Engineering Weyl phases and nonlinear Hall effects in T$_d$-MoTe$_2$, Phys. Rev. Lett. **125**, 046402 (2020).

[24] B. T. Zhou, C.-P. Zhang, and K. T. Law, Highly tunable nonlinear Hall effects induced by spin-orbit couplings in strained polar transition-metal dichalcogenides, Phys. Rev. Appl. **13**, 024053 (2020).

[25] Y. Gao, S. A. Yang, and Q. Niu, Field induced positional shift of Bloch electrons and its dynamical implications, Phys. Rev. Lett. **112**, 166601 (2014).

[26] Y. Gao, S. A. Yang, and Q. Niu, Geometrical effects in orbital magnetic susceptibility, Phys. Rev. B **91**, 214405 (2015).

[27] S. Lai, H. Liu, Z. Zhang, J. Zhao, X. Feng, N. Wang, C. Tang, Y. Liu, K. S. Novoselov, S. A. Yang *et al.*, Third-order nonlinear Hall effect induced by the Berry-connection polarizability tensor, Nat. Nanotechnol. **16**, 869 (2021).

[28] H. Liu, J. Zhao, Y.-X. Huang, X. Feng, C. Xiao, W. Wu, S. Lai, W.-b. Gao, and S. A. Yang, Berry connection polarizability tensor and third-order Hall effect, Phys. Rev. B **105**, 045118 (2022).

[29] X.-G. Ye, P.-F. Zhu, W.-Z. Xu, Z. Zang, Y. Ye, and Z.-M. Liao, Orbital polarization and third-order anomalous Hall effect in WTe$_2$, Phys. Rev. B **106**, 045414 (2022).

[30] C. Wang, R.-C. Xiao, H. Liu, Z. Zhang, S. Lai, C. Zhu, H. Cai, N. Wang, S. Chen, Y. Deng *et al.*, Room-temperature third-order nonlinear Hall effect in Weyl semimetal TaIrTe$_4$, Natl. Sci. Rev. **9**, nwac020 (2022).

[31] Z. Wang, H. Weng, Q. Wu, X. Dai, and Z. Fang, Three-dimensional Dirac semimetal and quantum transport in Cd$_3$As$_2$, Phys. Rev. B **88**, 125427 (2013).

[32] M. Neupane, S.-Y. Xu, R. Sankar, N. Alidoust, G. Bian, C. Liu, I. Belopolski, T.-R. Chang, H.-T. Jeng, H. Lin *et al.*, Observation of a three-dimensional topological Dirac semimetal phase in high-mobility Cd$_3$As$_2$, Nat. Commun. **5**, 3786 (2014).

[33] S. Jeon, B. B. Zhou, A. Gyenis, B. E. Feldman, I. Kimchi, A. C. Potter, Q. D. Gibson, R. J. Cava, A. Vishwanath, and A. Yazdani, Landau quantization and quasiparticle interference in the three-dimensional Dirac semimetal Cd$_3$As$_2$, Nat. Mater. **13**, 851 (2014).

[34] J. Xiong, S. K. Kushwaha, T. Liang, J. W. Krizan, M. Hirschberger, W. Wang, R. J. Cava, and N. P. Ong, Evidence for the chiral anomaly in the Dirac semimetal Na$_3$Bi, Science **350**, 413 (2015).

[35] H. Li, H. He, H.-Z. Lu, H. Zhang, H. Liu, R. Ma, Z. Fan, S.-Q. Shen, and J. Wang, Negative magnetoresistance in Dirac semimetal Cd$_3$As$_2$, Nat. Commun. **7**, 10301 (2016).

[36] C.-Z. Li, L.-X. Wang, H. Liu, J. Wang, Z.-M. Liao, and D.-P. Yu, Giant negative magnetoresistance induced by the chiral anomaly in individual Cd$_3$As$_2$ nanowires, Nat. Commun. **6**, 10137 (2015).

[37] Z. J. Xiang, D. Zhao, Z. Jin, C. Shang, L. K. Ma, G. J. Ye, B. Lei, T. Wu, Z. C. Xia, and X. H. Chen, Angular-dependent phase factor of Shubnikov–de Haas oscillations in the Dirac semimetal Cd$_3$As$_2$, Phys. Rev. Lett. **115**, 226401 (2015).

[38] L. P. He, X. C. Hong, J. K. Dong, J. Pan, Z. Zhang, J. Zhang, and S. Y. Li, Quantum transport evidence for the three-dimensional Dirac semimetal phase in Cd$_3$As$_2$, Phys. Rev. Lett. **113**, 246402 (2014).

[39] Y. Zhao, H. Liu, C. Zhang, H. Wang, J. Wang, Z. Lin, Y. Xing, H. Lu, J. Liu, Y. Wang *et al.*, Anisotropic Fermi surface and quantum limit transport in high mobility

three-dimensional Dirac semimetal Cd_3As_2, Phys. Rev. X **5,** 031037 (2015).

[40] C. M. Wang, H.-Z. Lu, and S.-Q. Shen, Anomalous phase shift of quantum oscillations in 3D topological semimetals, Phys. Rev. Lett. **117,** 077201 (2016).

[41] See Supplemental Material at http://link.aps.org/supplemental/10.1103/PhysRevLett.131.186302 for the numerical calculation of electric-field-induced Berry curvature dipole, frequency dependence of nonlinear Hall responses, results from another device, the general scaling law of nonlinear Hall signals, quantitative comparison of Berry curvature dipole from experimental and theoretical results, and numerical comparison with a topologically trivial insulator model, which includes Refs. [42,43].

[42] Z. Z. Du, C. M. Wang, S. Li, H.-Z. Lu, and X. C. Xie, Disorder-induced nonlinear Hall effect with time-reversal symmetry, Nat. Commun. **10,** 3047 (2019).

[43] J. Duan, Y. Jian, Y. Gao, H. Peng, J. Zhong, Q. Feng, J. Mao, and Y. Yao, Giant second-order nonlinear Hall effect in twisted bilayer graphene, Phys. Rev. Lett. **129,** 186801 (2022).

[44] I. Sodemann and L. Fu, Quantum nonlinear Hall effect induced by Berry curvature dipole in time-reversal invariant materials, Phys. Rev. Lett. **115,** 216806 (2015).

[45] C.-Z. Li, J.-G. Li, L.-X. Wang, L. Zhang, J.-M. Zhang, D. Yu, and Z.-M. Liao, Two-carrier transport induced Hall anomaly and large tunable magnetoresistance in Dirac semimetal Cd_3As_2 nanoplates, ACS Nano **10,** 6020 (2016).

[46] A.-Q. Wang, P.-Z. Xiang, X.-G. Ye, W.-Z. Zheng, D. Yu, and Z.-M. Liao, Room-temperature manipulation of spin texture in a Dirac semimetal, Phys. Rev. Appl. **14,** 054044 (2020).